Noncircular Measurement and Mitigation of I/Q Imbalance for OFDM-Based WLAN Transmitters

Zhe Li, *Student Member, IEEE,* Yili Xia, *Member, IEEE,* Wenjiang Pei, Kai Wang, Yongming Huang, *Member, IEEE,* and Danilo P. Mandic, *Fellow, IEEE*

***Abstract*— In future high-speed communication networks, the in-phase/quadrature (I/Q) imbalance mitigation and oscillator drift compensation is a key issue in the design of orthogonal frequency division multiplexing (OFDM)-based wireless LAN (WLAN) transmitters. To this end, we propose a two-stage I/Q imbalance measurement method, where by virtue of the WLAN standard-compliant training sequences, a coarse I/Q imbalance estimation is initially performed jointly with channel equalization. This makes it possible to decouple the effects of frequency-selective channels from the exact amplitude and phase imbalances induced by the local oscillator. Next, the so recovered symbols in *DATA* field of standardized OFDM systems, such as the IEEE 802.11ac, are recalibrated using a decision-directed scheme; this facilitates least squares-based fine I/Q imbalance estimation. For rigor, augmented complex statistics is employed to account for the effects of data noncircularity and widely linear natures of communication channels. Computer simulations and real world experiments based on the IEEE 802.11ac compliant signals demonstrate the high accuracy of the proposed technique for OFDM-based WLAN transmitters.**

***Index Terms*— in-phase/quadrature (I/Q) imbalance, orthogonal frequency division multiplexing (OFDM), RF measurements, transmitter testing, wireless LAN (WLAN).**

I. Introduction

ORTHOGONAL frequency division multiplexing (OFDM) techniques are widely adopted in current wireless LAN (WLAN) standards, such as the IEEE 802.11 a/g/n/ac [1]–[4]. An efficient implementation of such physical layers is challenging, owing to the problems arising from current consumer RF integrated circuits of the WLAN transmitter (TX). In particular, imperfections of local oscillators (LOs) in RF circuits, at the analog front end, cause the in-phase/quadrature (I/Q) imbalance which is characterized by differences in the amplitudes of I/Q oscillators, together with the phase shift from the nominal 90° [5]. The I/Q imbalance also introduces the so-called mirror frequency interference (MFI), which impairs the modulation accuracy of the transmitter RF signal and considerably degrades the overall performance of the transmission system. Critically, the impact of I/Q imbalance is more pronounced in systems which employ high-order modulations and high coding rates, this makes the effective I/Q imbalance measurement and troubleshooting a fundamental task in the design of high data-rate communication testing systems.

The LO-induced I/Q imbalances can be assumed constant over the signal bandwidth, while a transmitter may also exhibit frequency-selective I/Q imbalances, caused by a mismatch in the baseband reconstruction filters [6]. Due to the complexity of RF circuit design and fabrication, the effect of the LO-induced I/Q impairments is more significant than that of the I/Q imbalances caused by filter mismatch in baseband circuits [7]. Most current studies dealing with frequency-dependent I/Q impairments in transmitters [6], [8], [9] employ a feedback circuit from the RF to the baseband in TX, in order to perform an online calibration. Due to the complicated and frequency-dependent I/Q imbalance model, intertwined with the channel impulse responses of the transmitter and the auxiliary feedback loop, it is difficult to provide an explicit estimation on the exact degree of I/Q imbalance. However, from the point of view of chip manufacturers, it is desirable to separate the measurement and calibration stages so as to better understand the I/Q impairments within the transmitters under test. To that end, in this paper, we focus on the enhancement of measurements of LO-induced frequency-independent I/Q impairments at the instrumentation level.

Measurement methods for the evaluation of frequency-independent I/Q imbalance are extensively reported in the literature, and can be classified into envelope detector (ED)-based and demodulator-based, according to the detection types of the modulator output signal. In analog EDs, the detection can be aided by a series of auxiliary sinusoidal signals [10]–[12], or by access to the transmitted I/Q signals [13]. By using an ideal quadrature demodulator,

Manuscript received May 11, 2016; revised August 10, 2016; accepted September 26, 2016. Date of publication January 5, 2017; date of current version February 8, 2017. This work was supported in part by the National Natural Science Foundation of China under Grant 61271058 and Grant 61401094, in part by the Natural Science Foundation of Jiangsu Province under Grant BK20140645, in part by the Fundamental Research Funds for the Central Universities under Grant 2242016K41050, and in part by the Scientific Research Foundation for the Returned Overseas Chinese Scholars, State Education Ministry of China. The Associate Editor coordinating the review process was Dr. Matteo Pastorino. *(Corresponding author: Yili Xia.)*

Z. Li, Y. Xia, W. Pei, K. Wang, and Y. Huang are with the School of Information Science and Engineering, Southeast University, Nanjing 210096, China (e-mail: lizhe_nanjing@seu.edu.cn; yili_xia@seu.edu.cn; wjpei@seu.edu.cn; kaiwang@seu.edu.cn; huangym@seu.edu.cn).

D. P. Mandic is with the Department of Electrical and Electronic Engineering, Imperial College London, London SW7 2AZ, U.K. (e-mail: d.mandic@imperial.ac.uk).

Color versions of one or more of the figures in this paper are available online at http://ieeexplore.ieee.org.

Digital Object Identifier 10.1109/TIM.2016.2639778

a clustering-based method in [14] detects the I/Q impairments of the modulator and consists of three stages: signal demodulation, constellation clustering (to match each I/Q diagram symbol to its ideal position), and evaluation of the amount of impairment. However, this method cannot be directly applied to multicarrier OFDM transmitters. An analytical model which accounts for the way I/Q impairments affect the RF output signal was proposed in [15] in the context of generic OFDM transmitters. An approach that extracts data with asymptotic amplitude normalization was discussed in [16] for OFDM WiMAX standard-compliant transmitters. Most quadrature demodulator-based methods discussed earlier, perform channel equalization before I/Q imbalance estimation, which implicitly assumes an ideal baseband measurement channel. However, in a real world I/Q measurement setup: 1) the physical channel connecting the transmitters under test and the measurement testbed, e.g., a vector signal analyzer (VSA) [17], is usually connected via a coaxial cable; 2) the perfect reconstruction low-pass filters in I/Q branches of transmitter–receiver chain often require linear-phase for zero intersymbol interference; these result in a frequency-selective channel impulse response [18]. Consequently, at instrumentation level for wideband multicarrier systems, the I/Q imbalance distortion introduced by the channel varies for different subcarriers. It is therefore desirable to perform joint I/Q imbalance measurement and channel equalization, so as to remove the channel effect from the measured I/Q imbalance within transmitters.

Recently, the blind I/Q imbalance estimation/compensation methods based on the second-order signal statistics have become particularly attractive, due to their relatively low implementation complexity. Based on the proper (second-order circular) statistical behavior of the desired signals [19]–[22], such methods include eigenvalue decomposition-assisted whitening transforms [23], block-based self-image cancellers [24], and adaptive filtering algorithms based on the widely linear estimation model [25]. Despite the potentially high I/Q compensation accuracy, such methods are associated with the amplitude and phase ambiguities. This is because the main aim of I/Q imbalance compensation is to eliminate the MFI component from the I/Q imbalanced transceiver signal. However, the MFI-eliminated signal is a complex-valued scaled version of the I/Q imbalance-free (desired) transceiver signal, and this complex-valued scaling factor introduces both amplitude scaling and phase rotation effects on the constellation mapping. By taking into consideration, the frequency-selective nature of the baseband equivalent channel, standard second-order signal statistics cannot provide enough degrees of freedom to estimate this complex-valued scaling factor, which in fact contains useful information on both the amplitude and phase imbalances; we therefore need to design enhanced methods for exact I/Q imbalance measurement at the transmitter side.

In this paper, we propose a two-stage framework for the I/Q imbalance measurement at the instrumentation level of OFDM-based WLAN transmitters. In the initial stage, a block-based blind method, which fully exploits the available second-order signal statistics, is proposed. Then, making use of the WLAN standard-compliant training sequences, coarse I/Q imbalance estimation is performed jointly with channel equalization in order to decouple the effects of baseband measurement channel on the exact amplitude and phase imbalances induced by the LO. Finally, the initially recovered symbols in *DATA* field of standardized OFDM systems, such as the IEEE 802.11ac, are recalibrated using a standard decision-directed scheme, which facilitates fine I/Q imbalance estimation. The performance of the proposed I/Q imbalance measurement method is assessed through numerical simulations and real world experiments at the instrumentation level. This yields performance advantages over the least squares (LSs) method [26] for OFDM-based WLAN transmission systems, especially when higher order modulation and coding schemes (MCSs) are employed. The main contributions of this paper are: 1) unlike the existing demodulator-based I/Q imbalance measurement/troubleshooting methods [14]–[16], [27], the equivalent baseband measurement channel is considered to be frequency-selective, which represents a more practical and generic measurement scenario; 2) apart from the commonly used the second-order circularity (properness) condition [24], we make use of the full second-order statistics of the desired signal by considering the pseudocross correlation between a subcarrier and its mirror frequency counterpart within OFDM transmission systems.

The rest of this paper is organized as follows. Section II gives a brief on the mathematical modeling of I/Q imbalances in OFDM-based WLAN transmitters and the full second-order statistics of complex-valued random signals. The proposed method is described in Section III. Simulations and real world measurement experiments are given in Sections IV-A and IV-B, respectively. Section V concludes this paper.

II. Preliminaries

A. I/Q Imbalances in OFDM-Based WLAN Transmitters

Within the OFDM-based transmitters, frequency-independent I/Q imbalances induced by the LO are a major obstacle in practical transmitter calibration. Fig. 1 shows a typical I/Q imbalanced transmitter, where the relative amplitude and phase imbalances between the I and Q channels are denoted by g and θ, and represent mismatches of the quadrature mixer circuit. The discrete-time baseband equivalent modulator output signal $x(n)$ is then typically of the form [24]

$$x(n) = \beta s(n) + \alpha s^*(n) + d \tag{1}$$

where $s(n)$ denotes the discrete-time desired (I/Q imbalance-free) baseband waveform, d is the dc-offset component, and β and α are, respectively, defined as

$$\begin{aligned} \beta &= 1/2(1 + ge^{-j\theta}) \\ \alpha &= 1/2(1 - ge^{-j\theta}). \end{aligned} \tag{2}$$

Note that due to the complex-valued nature of β and α, the exact values of both the amplitude and phase imbalances g and θ can be directly calculated through a ratio between β and α, e.g., $(\beta)/(\alpha)$, instead of using their exact values.

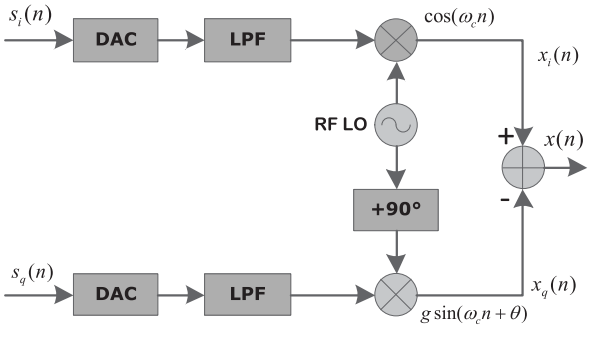

Fig. 1. Architecture of an I/Q imbalanced modulator.

B. Second-Order Signal Statistics

Since in OFDM systems, the output signals are transmitted by blocks, it is natural to interpret the imbalance model in (1) in the frequency domain, to yield

$$X_k(m) = \beta S_k(m) + \alpha S^*_{-k}(m) \quad (k \neq 0) \tag{3}$$

where k and m refer, respectively, to the subcarrier index and baseband OFDM symbol index, $S_k(m)$ represents the desired data on subcarrier k within the mth baseband OFDM symbol, and $X_k(m)$ is the resulting observation of $S_k(m)$, affected by the I/Q imbalance.[1]

We follow the standard assumptions that the desired signal $S_k(m)$ is a zero-mean ergodic proper random process with equal variances, σ_s^2, in each subcarrier k, for which the distribution exhibits circular symmetry (i.e., $E[S_k(m)S_k(m)] = 0$) [19]. The second-order circularity (properness) assumption is valid in most cases within OFDM-based WLAN standard family based on complex-valued modulations, such as the M-quadrature-amplitude modulation (QAM) used in the IEEE 802.11 a/g/n/ac [1]–[4]. Furthermore, in such cases, there exists no mutual dependence between the transmitted signals in the subcarrier and its mirror frequency counterpart, i.e., $E[S_k(m){S_k}^*(m)] = E[S_{-k}(m){S_{-k}}^*(m)] = \sigma_s^2$ and $E[S_k(m)S_{-k}(m)] = 0$ [28]. Then, from (3), the autocorrelation at subcarriers k and $-k$ is given by

$$\begin{aligned} E[X_k(m)X^*_k(m)] &= E[X_{-k}(m)X^*_{-k}(m)] \\ &= (|\beta|^2 + |\alpha|^2)\sigma_s^2 \end{aligned} \tag{4}$$

and the pseudocross correlation by

$$E[X_k(m)X_{-k}(m)] = 2\beta\alpha\sigma_s^2. \tag{5}$$

Note that this pseudocross correlation vanishes only when the modulator output is I/Q imbalance-free, i.e., $\alpha = 0$ in (3), this will play a key role in the proposed I/Q imbalance measurement framework.

[1]Note that, compared with (1), the dc-offset component d has been removed from the analysis, since the subcarrier 0 has been selected as one of the null-subcarriers in OFDM-based WLAN standards due to practical implementation issues.

III. Proposed Second-Order Statistics-Based I/Q Imbalance Measurement

In wireless indoor or outdoor communication scenarios, the transmission channel is usually considered as a wide-sense stationary uncorrelated scattering random process, and hence, its impulse response is usually assumed to be time varying and exposed to frequency-selective fading. Therefore, the properness (second-order circularity) assumption on the received signal is always valid, no matter whether the transmitted signal $X_k(m)$ is proper or not. In other words, a time varying fading channel actually reinforces the proper nature of a signal [25]. However, in real world I/Q imbalance measurement setups for OFDM-based WLAN transmitters, the physical channel connecting transmitters under test and the measurement test bed, e.g., a VSA [17], is usually in the form of a coaxial cable, while other RF or baseband components in the transmitter–receiver chain are considered relatively time-invariant within one OFDM transmission frame. Moreover, the perfect reconstruction low-pass filters in the I/Q branches of the transmitter–receiver chain often require linear phase for zero intersymbol interference, resulting in a frequency-selective channel for the measurement [18]. As a result, in wideband multicarrier systems, the time-invariant and frequency-selective property of the channel impulse response still maintains the impropriety of the transmitted I/Q imbalanced signals [23], but the impropriety-related distortion by the frequency-selective channel varies for different subcarriers. Therefore, it is desirable to perform joint I/Q imbalance measurement and channel equalization so as to decouple the channel effect from the exact I/Q imbalance amount within transmitters.

A. Baseband Signal Preprocessing

In order to retrieve the baseband components of the modulator output signals at a testbed, e.g., a VSA, several signal preprocessing operations need to be performed, according to standard requirements. As shown in Fig. 2, the initial operations for the acquisition of the baseband components include power triggering, automatic gain control (AGC), resampling, and subframe recognition [16]. The data acquisition is triggered when the received power exceeds a reference threshold. An AGC algorithm is then used to adjust both the low noise and variable gain amplifiers in AGC circuits in order to maintain the same level of amplification for input signals. An ordinary digital resampling algorithm is then applied on both the I/Q components, extracted by the analog-to-digital converter, in order to ensure that the sampling rate is equal to an integer multiple of the generation frequency given by the standard. After the resampling operation, the beginning and the end of each subframe within the acquired signal are detected by searching for the gap that separates each two successive subframes. The signal is next downsampled to the nominal generation frequency, and partitioned into a series of OFDM symbols. After discarding the cyclic prefix within the OFDM symbols, a transformation into the frequency domain is performed using Fast Fourier Transform (FFT). Note that before we start joint I/Q and channel estimation, the training sequences in the first several OFDM symbols, i.e., the

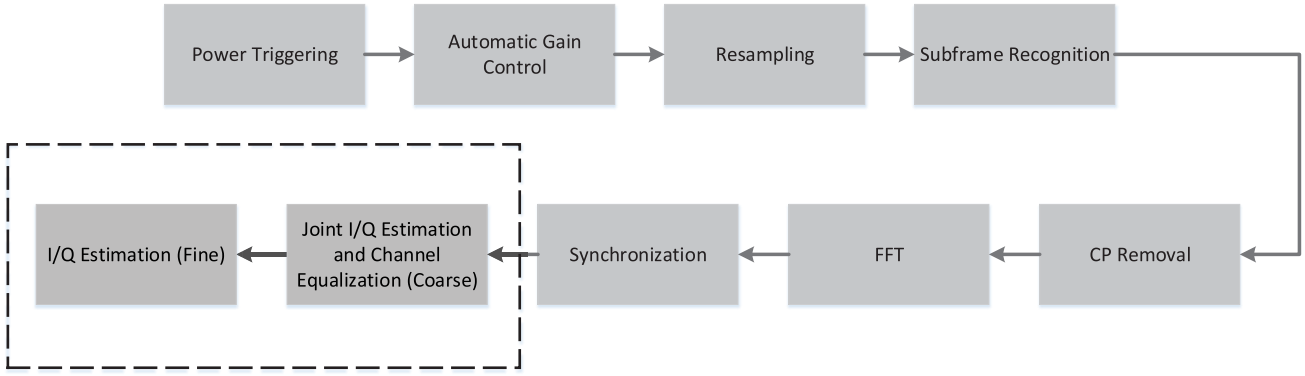

Fig. 2. Flowchart of the proposed I/Q measurement methodology.

PREAMBLE field, are used to synchronize frequency/timing errors [29].

By taking into consideration the channel and noise effects, the received discrete-time baseband signal at the measurement testbed can be described in the frequency domain as

$$Y_k(m) = H_k[\beta S_k(m) + \alpha S^*_{-k}(m)] + U_k(m) \tag{6}$$

where H_k is the frequency-selective channel impulse response at the subcarrier k, and $U_k(m)$ is assumed to be the zero-mean white Gaussian noise with equal variance σ_u^2 for all subcarriers.

B. Joint Coarse I/Q Imbalance Estimation and Channel Equalization

To give a clear illustration of the proposed method, we choose 802.11ac 80-MHz very high throughput (VHT) waveforms [4] as an example; other OFDM-based WLAN standards, such as the IEEE 802.11a/g/n, are also applicable. The VHT long training field (VHT-LTF) occupies a total 242 subcarriers out of 256, that is, $\{\pm 2, \pm 3, \ldots, \pm 122\}$, while $\{-128 \sim -123, 123 \sim 127\}$ and $\{\pm 1, 0\}$ are reserved as guard band and center subcarriers, respectively. The VHT short training field (VHT-STF) is four times downsampled compared with VHT-LTF, occupying only 48 tones. In *DATA* field, the collection of data subcarriers are almost the same as those of VHT-LTF subcarriers, except $\{\pm 11, \pm 39, \pm 75, \pm 103\}$, which are used as pilot subcarriers. We shall denote the three subcarrier collections of VHT-LTF, VHT-STF, and *DATA* field as $C_{VHT-LTF}$, $C_{VHT-STF}$, and C_{DATA}, respectively.

Using $Y_k(m)$ to represent received data in *DATA* field on subcarrier k, from (6), we can now obtain the conjugate of received data on mirror subcarrier $-k$ as

$$Y^*_{-k}(m) = H^*_{-k}[\beta^* S^*_{-k}(m) + \alpha^* S_k(m)] + U^*_{-k}(m). \tag{7}$$

Define

$$\lambda_{1,k} = \frac{\alpha H_k}{\beta^* H^*_{-k}} \tag{8}$$

and by observing that the mirror frequency term in (6) can be suppressed by subtracting $Y^*_{-k}(m)$ multiplied by λ_1, this yields

$$\begin{aligned} Z_k(m) &= Y_k(m) - \lambda_{1,k} Y^*_{-k}(m) \\ &= w_{1,k} S_k(m) + U_k(m) - \lambda_{1,k} U^*_{-k}(m) \end{aligned} \tag{9}$$

where

$$w_{1,k} = \frac{|\beta|^2 - |\alpha|^2}{\beta^*} H_k \tag{10}$$

and $Z_k(m)$ is the data on subcarrier k with eliminated MFI.

In a similar way, the conjugate of the signal on subcarrier $-k$, with removed MFI, can be derived as

$$\begin{aligned} Z^*_{-k}(m) &= Y^*_{-k}(m) - \lambda_{2,k} Y_k(m) \\ &= w_{2,k} S^*_{-k}(m) + U^*_{-k}(m) - \lambda_{2,k} U_k(m) \end{aligned} \tag{11}$$

where

$$\lambda_{2,k} = \frac{\alpha^* H^*_{-k}}{\beta H_k} \tag{12}$$

and

$$w_{2,k} = \frac{|\beta|^2 - |\alpha|^2}{\beta} H^*_{-k}. \tag{13}$$

From the analysis in (9) and (11), in order to extract the estimate $\hat{S}_k(m)$ which is equalized and with removed I/Q imbalance, we need appropriate estimates for $\lambda_{1,k}$, $\lambda_{2,k}$, $w_{1,k}$, and $w_{2,k}$. This will allow us to compute the exact amounts of amplitude/phase imbalances from (3), since

$$\begin{aligned} \gamma &= \frac{\beta}{\alpha} \\ &= \frac{w_{1,k}}{w_{2,k}\lambda_{1,k}} \quad \text{or} \quad \left(\frac{w_{2,k}}{w_{1,k}\lambda_{2,k}}\right)^*. \end{aligned} \tag{14}$$

A straightforward estimation on $w_{1,k}$ and $w_{2,k}$ can be achieved by using (9) and the VHT-LTF part of received signal at a VSA, as

$$\begin{aligned} \hat{w}_{1,k} &= \frac{Z_{k,VHT-LTF}}{S_{k,VHT-LTF}} = \frac{Y_{k,VHT-LTF} - \hat{\lambda}_{1,k} Y^*_{k,VHT-LTF}}{S_{k,VHT-LTF}} \\ \hat{w}_{2,k} &= \hat{w}^*_{1,-k}, \quad k \in C_{DATA}. \end{aligned} \tag{15}$$

To obtain $\hat{\lambda}_{1,k}$ or $\hat{\lambda}_{2,k}$, we here propose a novel blind method which exploits the full second-order statistics of $Y_k(m)$ and its mirror frequency counterpart $Y_{-k}(m)$. For the received signals in *DATA* field, the second-order moments of $Y_k(m)$ and $Y_{-k}(m)$, denoted as a and b, respectively, are defined as

$$a = E[Y_k(m)Y^*_k(m)] = (|\beta|^2 + |\beta|^2)|H_k|^2\sigma_s^2 + \sigma_u^2 \tag{16}$$

$$b = E[Y_{-k}(m)Y^*_{-k}(m)] = (|\beta|^2 + |\beta|^2)|H_{-k}|^2\sigma_s^2 + \sigma_u^2. \tag{17}$$

Since high signal-to-noise ratio (SNR) conditions are expected at the VSA side at the instrumentation level, to remove the noise terms in both (16) and (17), we calculate

$$a \approx (|\beta|^2 + |\beta|^2)|H_k|^2\sigma_s^2 \tag{18}$$
$$b \approx (|\beta|^2 + |\beta|^2)|H_{-k}|^2\sigma_s^2. \tag{19}$$

In addition, due to the impropriety of the modulator outputs at the transmitter, that is, $X_k(m)$ and $X_{-k}(m)$, the pseudocross correlation between the received signal $Y_k(m)$ and its mirror frequency counterpart $Y_{-k}(m)$ does exist, which provides us with another degree of freedom to access the second-order statistical behavior, denoted by c and given by

$$c = E[Y_k(m)Y_{-k}(m)] = 2\beta\alpha H_k H_{-k}\sigma_s^2. \tag{20}$$

We can now define a new parameter

$$p = \frac{|c|^2}{ab} \tag{21}$$

which, according to (18)–(20), can be further evaluated as

$$p = \frac{4|\beta|^2|\alpha|^2|H_k|^2|H_{-k}|^2\sigma_s^4}{(|\beta|^2 + |\alpha|^2)^2|H_k|^2|H_{-k}|^2\sigma_s^4} = \frac{4|\beta|^2|\alpha|^2}{(|\beta|^2 + |\alpha|^2)^2}. \tag{22}$$

Upon substituting $\gamma = \frac{\beta}{\alpha}$ into (22), and after a few mathematical manipulations, a fourth-order equation in $|\gamma|$ is obtained as

$$p|\gamma|^4 + (2p - 4)|\gamma|^2 + p = 0. \tag{23}$$

Solving (23) for $|\gamma|$, and considering that $|\gamma| \geq 0$, we obtain two solutions

$$|\gamma_1| = \sqrt{\frac{(2 + 2\sqrt{1-p})}{p}} - 1, |\gamma_2| = \sqrt{\frac{(2 - 2\sqrt{1-p})}{p}} - 1. \tag{24}$$

A feasible choice between the two solutions of $|\gamma|$ is obtained in the following.

Lemma 1: The range for $|\gamma|$ is $|\gamma| > 1$ for all practical values of $|\theta| < \pi/2$.

Proof: Using the definitions of β and α in (2), we have $|\beta|^2 = 1 + g^2 + 2g\cos(\theta)$ and $|\alpha|^2 = 1 + g^2 - 2g\cos(\theta)$. This proves the lemma, because $\cos(\theta) > 0$ for $|\theta| < \pi/2$, and hence, $|\beta| > |\alpha|$ and $|\gamma| > 1$. □

Lemma 2: The ranges for $|\gamma_1|$ and $|\gamma_2|$ are $|\gamma_1| \geq 1$ and $|\gamma_2| \leq 1$.

Proof: First, according to (23), $|\gamma_1|^2$ and $|\gamma_2|^2$ are reciprocal pairs, i.e., $|\gamma_2|^2 = 1/|\gamma_1|^2$, and so are $|\gamma_1|$ and $|\gamma_2|$, meaning that either $|\gamma_1| \geq 1$ and $|\gamma_2| \leq 1$, or $|\gamma_1| \leq 1$ and $|\gamma_2| \geq 1$. Then, from (21), observe that $0 < p \leq 1$, since

$$ab = (|\beta|^2 + |\beta|^2)^2|H_k|^2|H_{-k}|^2\sigma_s^4 \geq 4|\beta|^2|\beta|^2|H_k|^2|H_{-k}|^2\sigma_s^4 = |c|^2. \tag{25}$$

Consider now the derivative of $|\gamma_1|^2$ with respect to p, given by

$$\frac{d|\gamma_1|^2}{dp} = \frac{-1}{\sqrt{1-p}} - \frac{2 + 2\sqrt{1-p}}{p^2} = \frac{-(1-p)^2 - 2\sqrt{1-p} - 1}{p^2\sqrt{1-p}}. \tag{26}$$

For $p \in (0, 1)$, $(d|\gamma_1|^2)/(dp) < 0$, $|\gamma_1|^2$ is a monotonous decreasing function of p, for which the minimum value is 1 only if $p = 1$. Therefore, $|\gamma_1| \geq 1$, and hence, $|\gamma_2| \leq 1$ □

From Lemmas 1 and 2, it can be concluded that the feasible solution for $|\gamma|$ is $|\gamma_1|$, is given by

$$|\gamma| = \sqrt{\frac{(2 + 2\sqrt{1-p})}{p}} - 1. \tag{27}$$

Subsequently, $\lambda_{1,k}$ and $\lambda_{2,k}$ can be expressed as

$$\lambda_{1,k} = \frac{1}{2}\left(1 + \frac{1}{|\gamma|^2}\right)\frac{c}{b} \tag{28}$$
$$\lambda_{2,k} = \frac{1}{2}\left(1 + \frac{1}{|\gamma|^2}\right)\left(\frac{c}{a}\right)^*. \tag{29}$$

Now that $|\gamma|$, $\lambda_{1,k}$, and $\lambda_{2,k}$ have been expressed as a function of the ensemble averages a, b, and c, their estimates based on a single realization of the signals $\{Y_k(m) \mid m = 0, 1, \ldots, M-1\}$ and $\{Y_{-k}(m) \mid m = 0, 1, \ldots, M-1\}$ can be derived by exploiting the ergodic property of $X_k(m)$ and $X_{-k}(m)$. We are, therefore, able to obtain consistent mean square estimators for a, b, and c in the form

$$\hat{a}_M = \frac{1}{M}\sum_{m=0}^{M-1}|Y_k(m)|^2$$
$$\hat{b}_M = \frac{1}{M}\sum_{m=0}^{M-1}|Y_{-k}(m)|^2$$
$$\hat{c}_M = \frac{1}{M}\sum_{m=0}^{M-1}Y_k(m)Y_{-k}(m) \tag{30}$$

where M represents the total number of received OFDM symbols in *DATA* field. Then, as $X_k(m)$ and $X_{-k}(m)$ are ergodic in a wide sense, so are $Y_k(m)$, $Y_{-k}(m)$, $|Y_k(m)|^2$, $|Y_{-k}(m)|^2$, and $Y_k(m)Y_{-k}(m)$; thus, $\lim_{M\to\infty}\hat{a}_M = a$, $\lim_{M\to\infty}\hat{b}_M = b$, and $\lim_{M\to\infty}\hat{c}_M = c$. Therefore, $\hat{\lambda}_{1,k}$ and $\hat{\lambda}_{2,k}$ can be explicitly estimated as

$$\hat{\lambda}_{1,k} = \frac{\hat{c}_M\left(1 + \sqrt{1 - \frac{|\hat{c}_M|^2}{\hat{a}_M\hat{b}_M}}\right)}{\hat{b}_M\left(2 + 2\sqrt{1 - \frac{|\hat{c}_M|^2}{\hat{a}_M\hat{b}_M}} - \frac{|\hat{c}_M|^2}{\hat{a}_M\hat{b}_M}\right)} \tag{31}$$

$$\hat{\lambda}_{2,k} = \frac{\hat{c}_M^*\left(1 + \sqrt{1 - \frac{|\hat{c}_M|^2}{\hat{a}_M\hat{b}_M}}\right)}{\hat{a}_M^*\left(2 + 2\sqrt{1 - \frac{|\hat{c}_M|^2}{\hat{a}_M\hat{b}_M}} - \frac{|\hat{c}_M|^2}{\hat{a}_M\hat{b}_M}\right)} \tag{32}$$

and we have $\lim_{M\to\infty}\hat{\lambda}_{1,k} = \lambda_{1,k}$ and $\lim_{M\to\infty}\hat{\lambda}_{2,k} = \lambda_{2,k}$ [30]. Now, with $\hat{w}_{1,k}$, $\hat{w}_{2,k}$, $\hat{\lambda}_{1,k}$, and $\hat{\lambda}_{2,k}$ in hand, coarse estimation of γ can be achieved using (14), and from (9),

the signal in *DATA* field, $\hat{S}_k(m)$, which is channel equalized and with coarsely removed MFI, can be obtained as

$$\hat{S}_k(m) = \frac{Y_k(m) - \hat{\lambda}_{1,k} Y^*_{-k}(m)}{\hat{w}_{1,k}}. \tag{33}$$

C. Fine I/Q Imbalance Estimation

In order to enhance measurement accuracy based on the initial estimates, we can now apply the standard hard-decision detection [16], [26] on $\hat{S}_k(m)$ to obtain the recovered signal $\tilde{S}_k(m)$ according to the constellation mapping, which will be reused for fine I/Q imbalance estimation. Define the received signal vector in *DATA* field as

$$\mathbf{y}_k = [Y_k(0), Y_k(1), \ldots, Y_k(M)]^T \tag{34}$$

and the demodulated data matrix as

$$\tilde{\mathbf{S}}_k = \begin{bmatrix} \tilde{S}_k(0) & \tilde{S}^*_{-k}(0) \\ \tilde{S}_k(1) & \tilde{S}^*_{-k}(1) \\ \vdots & \vdots \\ \tilde{S}_k(M-1) & \tilde{S}^*_{-k}(M-1) \end{bmatrix} \tag{35}$$

to give

$$\mathbf{y}_k = \tilde{\mathbf{S}}_k \mathbf{g}_k \tag{36}$$

where $\mathbf{g}_k$ is the joint I/Q imbalance and channel impulse response parameter vector, defined as $\mathbf{g}_k = [\beta H_k, \alpha H_k]^T$, for which the optimal estimator in the LSs sense is given by

$$\hat{\mathbf{g}}_k = (\tilde{\mathbf{S}}_k^H \tilde{\mathbf{S}}_k)^{-1} \tilde{\mathbf{S}}_k^H \mathbf{y}_k \tag{37}$$

and a fine estimator of γ as

$$\hat{\gamma} = \frac{1}{234} \sum_{k \in C_{DATA}} \frac{\hat{\mathbf{g}}_k(1)}{\hat{\mathbf{g}}_k(2)} \tag{38}$$

where 234 is the total number of available subcarriers in C_{DATA}, and the fine-estimated I/Q amplitude and phase imbalances, that is, $\hat{g}$ and $\hat{\theta}$, can be obtained using the definition $\gamma = (\beta)/(\alpha)$ and (2), since

$$\gamma = \frac{\beta}{\alpha} = \frac{1 + g e^{-j\theta}}{1 - g e^{-j\theta}}. \tag{39}$$

IV. Simulations and Experimental Results

In order to illustrate the performance of the proposed I/Q imbalance measurement method, simulations in the MATLAB programming environment and real world experiments were conducted. For comparison, a standard-compliant block-based I/Q imbalance estimation technique from the literature was also considered [26]. This method, called the post-FFT LSs, was originally designed for I/Q imbalance measurement for OFDM receivers and has been merely customized for OFDM transceivers by considering a different mathematical model of I/Q imbalance to calculate the amplitude imbalance g and the phase imbalance θ using (2), as compared with the one used for OFDM receivers. This method has a similar implementation as the proposed one. The difference lies in the proposed joint I/Q and channel estimation step, where LSs are performed with the aid of a training sequence. However, since the standard dedicated training sequence VHT-STF occupies only a subgroup of the subcarriers, in order to equalize the received OFDM symbols in the *DATA* field, interpolation and extrapolation on the estimated channel impulse response are required within the fine I/Q imbalance estimation step. For more detail on its implementation, we refer to [26].

A. Computer Simulations

We first simulated an OFDM-based WLAN transmission system fully compliant with the IEEE 802.11 ac. The discrete baseband waveform $s(n)$ was generated with the following system parameters: length of subcarriers $K = 256$, length of cyclic prefix $K_{\text{cp}} = 64$, waveform bandwidth $B_c = 80$ MHz, and therefore, the OFDM symbol duration $T_{\text{sym}} = (K + K_{\text{cp}})/B_c = 4\ \mu s$, and guard interval $T_g = K_{\text{cp}}/B_c = 0.8\ \mu s$. The amplitude and phase mismatches imposed on $s(n)$ were set to $g = 1.3$ and $\theta = 7°$. The transmission channel considered was a three-tap multipath static-Rayleigh channel with frequency selectivity, where $h(n) = [0.866 + 0.5_J,\ 0.0643 + 0.0766_J,\ 0.0098 - 0.0017_J]$ (symbol period spacing) [31], and different levels of the white Gaussian noise $u(n)$ were added.

In the coarse estimation stage, the proposed method employed $M = 3000$ OFDM symbols in *DATA* field to calculate the full second-order statistics of the received discrete-time baseband signal $Y_k(m)$ and its mirror frequency component $Y_{-k}(m)$, that is, $\hat{a}_M$, $\hat{b}_M$, and $\hat{c}_M$, as given in (30). These were employed for the estimation of $\hat{\lambda}_{1,k}$ from (31) along each subcarrier $k \in C_{DATA}$. By using the standard-compliant VHT-LTF part of received signal and $\hat{\lambda}_{1,k}$ in hand, we estimated the parameter $w_{1,k}$ according to (15), and subsequently the coarsely MFI-eliminated and channel-equalized signal $\hat{S}_k(m)$ from (33) for each subcarrier $k \in C_{DATA}$. In the fine estimation step, first 200 symbols of $\hat{S}_k(m)$ were recalibrated by a hard-decision detector to obtain the recovered signal $\tilde{S}_k(m)$. Next, from the recovered signal $\tilde{S}_k(m)$ and the received signal $Y_k(m)$, a fine measurement of $\hat{\gamma}$ was performed in the LS sense by using (37) and (38), and from (39), we obtained fine estimate of both the amplitude and phase imbalances.

The performance evaluation was performed through the estimation bias in both the amplitude and phase imbalances, quantified as

$$\Delta g = 20 \log_{10}\left(\frac{\hat{g} - g}{g}\right) \text{ and } \Delta\theta = 20 \log_{10}\left(\frac{\hat{\theta} - \theta}{\theta}\right) \tag{40}$$

where $\hat{g}$ and $\hat{\theta}$ are, respectively, the estimates of g and θ, obtained by averaging 1000 independent trails.

Two sets of simulations were carried out based on different constellation sizes. In the first one, a 64-QAM modulation scheme conforming with the MCS 5 of the IEEE 802.11ac standard was employed. As shown in Fig. 3(a) and (b), the estimation performances of the post-FFT LS method and the proposed second-order statistics-based one were similar in the high SNR region for the 64-QAM modulation scheme (MSC5), but the proposed method was able to more

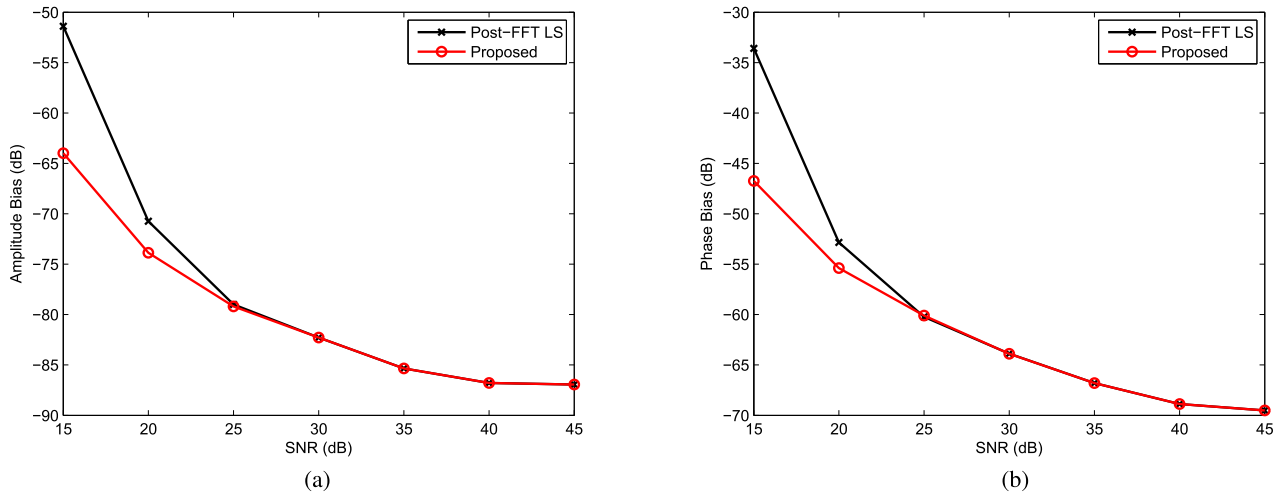

Fig. 3. Estimation performances of the post-FFT LS method [26] and the proposed method for a multipath (frequency selective) channel based on the IEEE 802.11ac 80-MHz 64-QAM modulation (MCS 5). (a) Amplitude bias $\triangle g$. (b) Phase bias $\triangle\theta$.

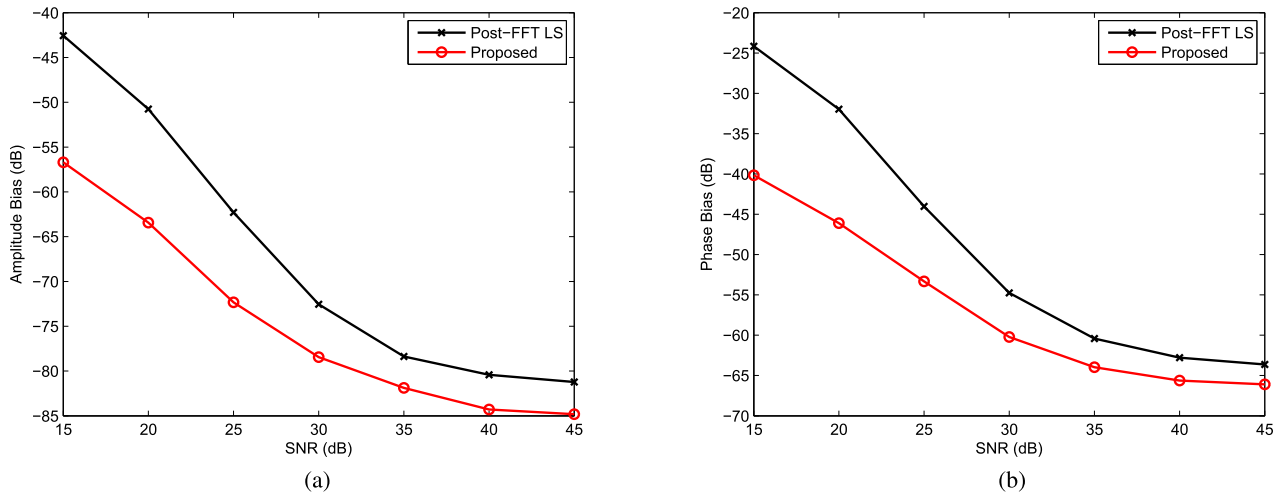

Fig. 4. Estimation performances of the post-FFT LS method [26] and the proposed method for a multipath (frequency selective) channel based on the IEEE 802.11ac 80-MHz 256-QAM modulation (MCS 8). (a) Amplitude bias $\triangle g$. (b) Phase bias $\triangle\theta$.

accurately estimate the I/Q impairment in both the amplitude and phase in the lower SNR region. This was mainly due to the fact that the required channel interpolation and extrapolation operations within the post-FFT LS method were sensitive to large noise levels. The proposed method can achieve direct channel equalization on each subcarrier in *DATA* field, which facilitates a more accurate hard-decision operation and was more accurate to extract recovered data for the subsequent fine I/Q imbalance estimation. As expected, these performance advantages were more pronounced when higher order MCSs were employed, e.g., a 256-QAM modulation (MCS 8), as shown in Fig. 4. However, we should mention that this enhanced reliability is achieved at a cost of increased computational complexity, because more observations are required to make the moment statistics in (30) mean square consistent. By considering Figs. 3 and 4, it is also interesting to observe that both methods gave better estimation of the amplitude imbalance g than the phase imbalance θ at the same SNR. This can be explained by Fig. 5, where as compared with $\triangle g$, $\triangle\theta$ was the major cause of estimation bias on γ, which is the key parameter to calculate $\hat{g}$ and $\hat{\theta}$ and was obtained by the proposed method in its fine I/Q imbalance estimation stage. This was also the case with the post-FFT LS method, and it may result from the nonlinear relationship of γ on g and θ, as given in (39).

B. Experimental Results

An experimental setup was developed to further evaluate the performance of the proposed second-order statistics-based I/Q imbalance measurement method. The measurement testbed built upon *Aeroflex* PXI modules is shown in Fig. 6, and the description of each PXI module is given in Table I. In the setup, the baseband I/Q waveforms were created by *Aeroflex IQ Creator* software running on a PC. The modulator output signals were then loaded into a nonvolatile memory of the vector signal generator (VSG). After low-pass filtering, the I/Q signal waveforms were fed to a quadrature modulator to

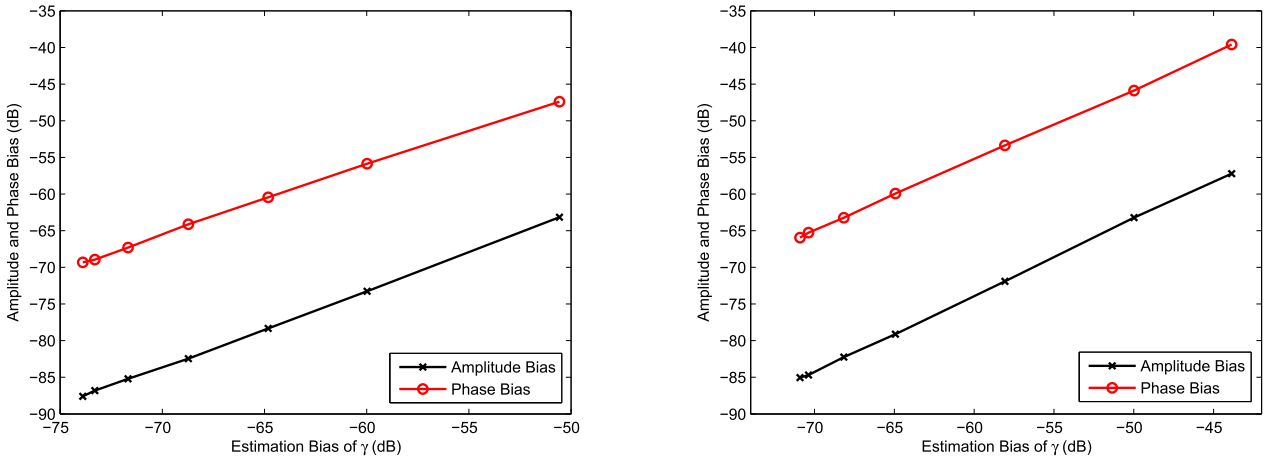

Fig. 5. Sensitivities of $\triangle g$ and $\triangle\theta$ versus $\triangle\gamma$ obtained by the proposed method at SNRs ranging from 15 to 45 dB. (a) 64-QAM modulation (MCS 5). (b) 256-QAM modulation (MCS 8).

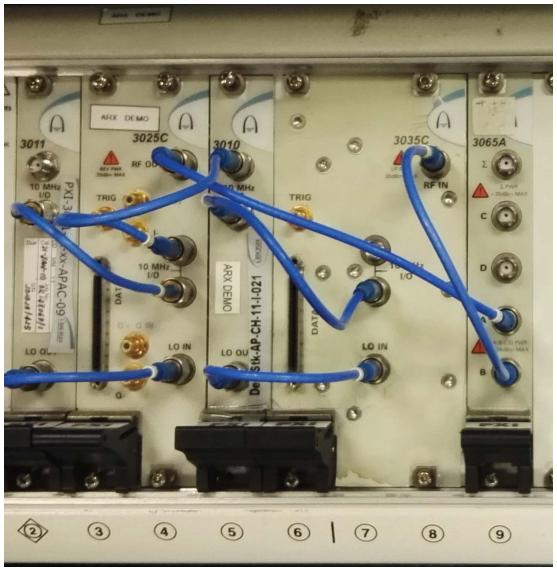

Fig. 6. I/Q imbalance measurement setup based on Aeroflex PXI modules.

TABLE I
DESCRIPTIONS OF AEROFLEX PXI MODULES

PXI-3025C	RF vector signal generator, with frequency range 1 MHz to 6 GHz , and signal bandwidth 90 MHz.
PXI- 3035C	RF vector signal analyzer, with frequency range 0.25 MHz to 6 GHz, and A/D bandwidth 90 MHz.
PXI-3011	RF synthesizer, providing 10 MHz reference for PXI-3025C
PXI-3010	RF synthesizer, providing 10 MHz reference for PXI-3035C.
PXI-3065A	RF switch and power loss combiner

TABLE II
ESTIMATED VARIANCES OF THE EQUIVALENT BASEBAND CHANNEL TRANSFER FUNCTION IN BOTH TIME AND FREQUENCY DOMAINS

time variation (per symbol period)	1.31×10^{-4}
frequency-selectivity (per subcarrier)	6.1×10^{-3}

generate a carrier-modulated RF signal at channel 36 (5.18 GHz). A VSA was used to detect the transmitted RF signal in a loopback way [32] and to down-converted it to baseband. After I/Q demodulation, complex-valued baseband data were transferred to the same PC, where I/Q imbalance estimation was implemented. Both the VSG and VSA were synchronized by the same 10-MHz reference clock. The RF output level of VSG was set to -10 dBm, and the reference level of VSA was set to 0 dBm. The OFDM system parameters, such as waveform bandwidth, OFDM symbol duration, and guard interval, were the same as those in the previous computer simulations. The sampling rate at the VSA side was $f_s = 160$ MHz.

Three types of signals, fully compliant with the IEEE 802.11ac 80 MHz, were generated. The first one employed a low density QPSK modulation (MCS 1) without any I/Q imbalance, and was used to estimate the equivalent baseband channel effect at this instrumentation level measurement. The length of OFDM symbols in *DATA* field was set to 3000. These OFDM symbols were known to the VSA, and hence, a direct measurement of the channel impulse response could be performed, resulting in a 3000×234 channel transfer function matrix $\mathbf{H_{n,m}}$. We calculated the variances of the channel transfer function in both time (per symbol period) and frequency (per subcarrier) along the two dimensions of this matrix; the results are given in Table II. Observe that compared with the time variation, the frequency-selectivity in channel, which is further shown in Fig. 7, is the dominant effect. This observation justifies our frequency-selective assumption on the channel, and illustrates the suitability of

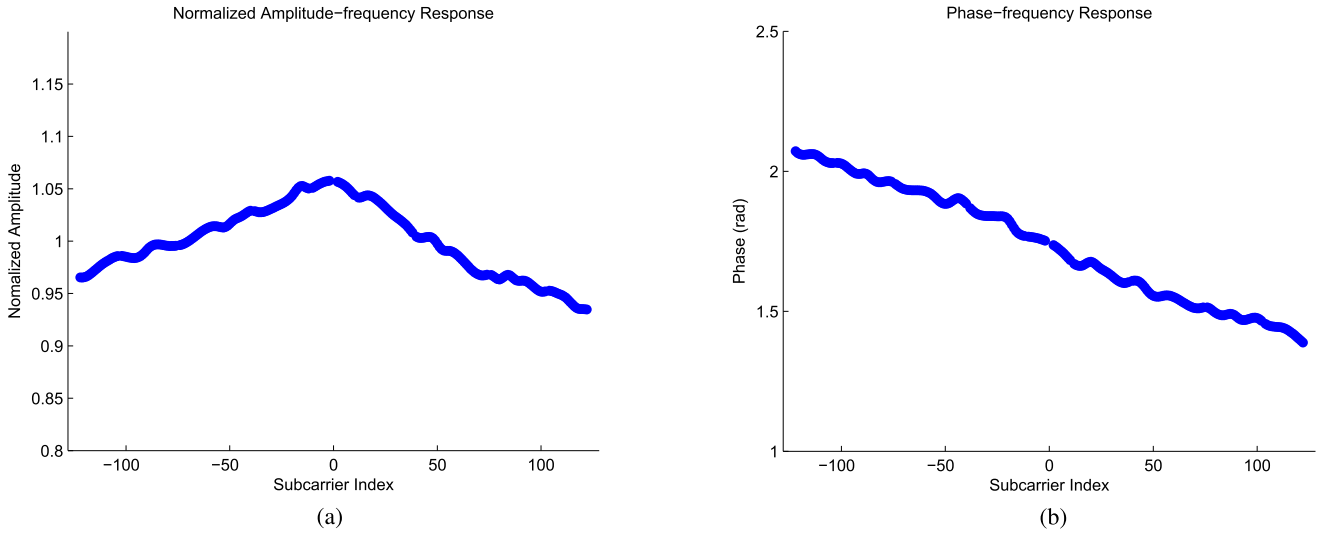

Fig. 7. Normalized channel impulse response per subcarrier spacing; the results were obtained by averaging 3000 OFDM symbols. (a) Normalized amplitude–frequency response of channel averaged in time. (b) Normalized phase–frequency response of channel averaged in time.

TABLE III
I/Q MEASUREMENT RESULTS

g	θ	64-QAM (MCS 5)				256-QAM (MCS 8)			
		Post-FFT LS		Proposed		Post-FFT LS		Proposed	
		Δg	$\Delta\theta$	Δg	$\Delta\theta$	Δg	$\Delta\theta$	Δg	$\Delta\theta$
-1 dB	1°	-52 dB	-41 dB	-52 dB	-41 dB	-51 dB	-33 dB	-53 dB	-40 dB
-1 dB	3°	-50 dB	-45 dB	-52 dB	-46 dB	-50 dB	-36 dB	-52 dB	-44 dB
-1 dB	5°	-50 dB	-49 dB	-51 dB	-50 dB	-50 dB	-41 dB	-51 dB	-48 dB
-3 dB	1°	-50 dB	-35 dB	-53 dB	-36 dB	-50 dB	-30 dB	-54 dB	-33 dB
-3 dB	3°	-52 dB	-40 dB	-53 dB	-40 dB	-51 dB	-35 dB	-53 dB	-37 dB
-3 dB	5°	-52 dB	-42 dB	-53 dB	-43 dB	-50 dB	-39 dB	-53 dB	-41 dB
-5 dB	1°	-53 dB	-30 dB	-54 dB	-30 dB	-51 dB	-27 dB	-54 dB	-29 dB
-5 dB	3°	-51 dB	-36 dB	-51 dB	-36 dB	-52 dB	-32 dB	-53 dB	-35 dB
-5 dB	5°	-50 dB	-38 dB	-54 dB	-39 dB	-52 dB	-33 dB	-54 dB	-36 dB

the proposed joint I/Q imbalance measurement and channel equalization scheme. It also indicates a potential way to improve the accuracy of I/Q imbalance measurement methods for transmitters [14]–[16], where an ideal baseband measurement channel is assumed. Note that although the channel impulse response is also assumed to be time-invariant, a slight fluctuation is inevitable in real world measurements.

In the next experiment, MCS 5 and MCS 8 modulated waveforms with different amounts of amplitude and phase imbalances were loaded into VSG. The measurement results are given in Table III. Again, observe that in all the cases the amplitude imbalance was more accurately estimated by both considered methods as compared with the phase imbalance. According to its specifications [33], for this experiment, the instrument was very likely to work in a high SNR environment. The performance advantages of the proposed second-order statistics-based method over the post-FFT LS method were not obvious for the 64-QAM modulation (MSC 5); however, the proposed method was able to more accurately estimate the impairment caused by the I/Q imbalance when higher order MCSs were employed, e.g., a 256-QAM modulation (MSC 8), with a 1–4 dB and 2–8 dB performance improvement in respective amplitude and phase imbalance estimation.

V. CONCLUSION

A novel two-stage I/Q imbalance measurement method for OFDM-based WLAN transmitters at the instrumentation level has been proposed. In the initial stage, the noncircular second-order statistics, assisted by the standard-compliant training sequences, has enabled the decoupling of the I/Q imbalance distortion from the effects of the measurement framework. This has made it possible to account for frequency selectivity of the channel at the instrumentation level for

wideband multicarrier systems. In the next stage, an enhanced I/Q imbalance measurement has been performed using a standard decision-directed scheme, in order to recalibrate the initially recovered symbols transmitted in *DATA* field of standardized OFDM systems. It has been further demonstrated through computer simulations and real world experiments on signals fully compliant with the IEEE 802.11 ac 80 MHz that the proposed method exhibits enhanced measurement robustness against both additive noise and frequency-selective transmission, as compared with the state-of-art post-FFT LS method. This advantage is more pronounced for higher order modulation schemes, such as the 256-QAM modulation (MSC 8).

REFERENCES

[1] *Part 11: Wireless LAN Medium Access Control (MAC) Physical Layer (PHY) Specifications High-Speed Physical Layer 5 GHz Band*, IEEE Standard 802.11a-1999, 1999.

[2] *Part 11: Wireless LAN Medium Access Control (MAC) Physical Layer (PHY) Specifications Amendment 4: Further Higher Data Rate Extension 2.4 GHz Band*, IEEE Standard 802.11g-2003, 2003.

[3] *Part 11: Wireless LAN Medium Access Control (MAC) Physical Layer (PHY) Specifications Amendment 5: Enhancements for Higher Thoughput*, IEEE Standard 802.11ac-2009, 2009.

[4] *Part 11:Wireless LAN Medium Access Control(MAC) Physical Layer (PHY) Sepcifications Amendment 4: Enhancements for Very High Throuput for Operation Bands Below 6GHz*, IEEE Standard 802.11ac-2013, 2013.

[5] B. Razavi, "Design considerations for direct-conversion receivers," *IEEE Trans. Circuits Syst. II, Analog Digit. Signal Process.*, vol. 44, no. 6, pp. 428–435, Jun. 1997.

[6] L. Anttila, M. Valkama, and M. Renfors, "Frequency-selective I/Q mismatch calibration of wideband direct-conversion transmitters," *IEEE Trans. Circuits Syst. II, Express Briefs*, vol. 55, no. 4, pp. 359–363, Apr. 2008.

[7] Z. Zhu, X. Huang, M. Caron, and H. Leung, "Blind self-calibration technique for I/Q imbalances and DC-offsets," *IEEE Trans. Circuits Syst. I, Reg. Papers*, vol. 61, no. 6, pp. 1849–1859, Jun. 2014.

[8] J. Luo, A. Kortke, W. Keusgen, and M. Valkama, "A novel adaptive calibration scheme for frequency-selective I/Q imbalance in broadband direct-conversion transmitters," *IEEE Trans. Circuits Syst. II, Express Briefs*, vol. 60, no. 2, pp. 61–65, Feb. 2013.

[9] Z. Zhu, X. Huang, and H. Leung, "Joint I/Q mismatch and distortion compensation in direct conversion transmitters," *IEEE Trans. Wireless Commun.*, vol. 12, no. 6, pp. 2941–2951, Jun. 2013.

[10] P. Handel and P. Zetterberg, "Receiver I/Q imbalance: Tone test, sensitivity analysis, and the universal software radio peripheral," *IEEE Trans. Instrum. Meas.*, vol. 59, no. 3, pp. 704–714, Mar. 2010.

[11] C. R. Rojas, P. Zetterberg, and P. Handel, "Transceiver inphase/quadrature imbalance, ellipse fitting, and the universal software radio peripheral," *IEEE Trans. Instrum. Meas.*, vol. 60, no. 11, pp. 3629–3639, Nov. 2011.

[12] V. Rampa, "I/Q compensation of broadband direct-conversion transmitters," *IEEE Trans. Wireless Commun.*, vol. 6, no. 13, pp. 3329–3342, Jun. 2014.

[13] R. Marchesani, "Digital precompensation of imperfections in quadrature modulators," *IEEE Trans. Commun.*, vol. 48, no. 4, pp. 552–556, Apr. 2000.

[14] L. Angrisani, M. D'Arco, and M. Vadursi, "Clustering-based method for detecting and evaluating I/Q impairments in radio-frequency digital transmitters," *IEEE Trans. Instrum. Meas.*, vol. 56, no. 6, pp. 2139–2146, Dec. 2007.

[15] L. Angrisani, I. Ghidini, and M. Vadursi, "A new method for I/Q impairment detection and evaluation in OFDM transmitters," *IEEE Trans. Instrum. Meas.*, vol. 55, no. 5, pp. 1480–1486, Oct. 2006.

[16] L. Angrisani, A. Napolitano, and M. Vadursi, "Measuring I/Q impairments in WiMAX transmitters," *IEEE Trans. Instrum. Meas.*, vol. 58, no. 5, pp. 1299–1306, May 2009.

[17] R. W. Lowdermilk and F. J. Harris, "Vector signal analyzer implemented as a synthetic instrument," *IEEE Trans. Instrum. Meas.*, vol. 58, no. 2, pp. 411–420, Feb. 2009.

[18] P. Siohan and F. M. D. Saint-Martin, "New designs of linear-phase transmitter and receiver filters for digital transmission systems," *IEEE Trans. Circuits Syst. II, Analog Digit. Signal Process.*, vol. 46, no. 4, pp. 428–433, Apr. 1999.

[19] B. Picinbono and P. Bondon, "Second-order statistics of complex signals," *IEEE Trans. Signal Process.*, vol. 45, no. 2, pp. 411–420, Feb. 1997.

[20] P. J. Schreier and L. L. Scharf, "Second-order analysis of improper complex random vectors and processes," *IEEE Trans. Signal Process.*, vol. 51, no. 3, pp. 714–725, Mar. 2003.

[21] D. P. Mandic and S. L. Goh, *Complex Valued Nonlinear Adaptive Filters: Noncircularity, Widely Linear and Neural Models*. Hoboken, NJ, USA: Wiley, 2009.

[22] Y. Xia, S. C. Douglas, and D. P. Mandic, "Adaptive frequency estimation in smart grid applications: Exploiting noncircularity and widely linear adaptive estimators," *IEEE Signal Process. Mag.*, vol. 29, no. 5, pp. 44–54, Sep. 2012.

[23] M. Valkama, M. Renfors, and V. Koivunen, "Blind signal estimation in conjugate signal models with application to I/Q imbalance compensation," *IEEE Signal Process. Lett.*, vol. 12, no. 11, pp. 733–736, Nov. 2005.

[24] G. T. Gil, "Nondata-aided I/Q mismatch and DC offset compensation for direct-conversion receivers," *IEEE Trans. Signal Process.*, vol. 56, no. 7, pp. 2662–2668, Jul. 2008.

[25] L. Anttila, M. Valkama, and M. Renfors, "Circularity-based I/Q imbalance compensation in wideband direct-conversion receivers," *IEEE Trans. Veh. Technol.*, vol. 57, no. 4, pp. 2099–2113, Jul. 2008.

[26] A. Tarighat, R. Bagheri, and A. H. Sayed, "Compensation schemes and performance analysis of IQ imbalances in OFDM receivers," *IEEE Trans. Signal Process.*, vol. 53, no. 8, pp. 3257–3268, Aug. 2005.

[27] L. Angrisani, M. D'Arco, and M. Vadursi, "Error vector-based measurement method for radiofrequency digital transmitter troubleshooting," *IEEE Trans. Instrum. Meas.*, vol. 54, no. 4, pp. 1381–1387, Aug. 2005.

[28] Y. Tsai, C. P. Yen, and X. Wang, "Blind frequency-dependent I/Q imbalance compensation for direct-conversion receivers," *IEEE Trans. Wireless Commun.*, vol. 9, no. 6, pp. 1976–1986, Jun. 2010.

[29] Q. Honglei, Q. Changquan, C. Li, and C. Yang, "Wireless LXI bus clock synchronization and triggering design," *IEEE Trans. Instrum. Meas.*, vol. 59, no. 9, pp. 2420–2430, Sep. 2010.

[30] G. H. Hardy, *A Course Pure Mathematics*. Cambridge, U.K.: Cambridge Univ. Press, 2005.

[31] J. J. de Witt and G.-J. van Rooyen, "A blind I/Q imbalance compensation technique for direct-conversion digital radio transceivers," *IEEE Trans. Veh. Technol.*, vol. 58, no. 4, pp. 2077–2082, May 2009.

[32] J.-S. Yoon and W. R. Eisenstadt, "Embedded loopback test for RF ICs," *IEEE Trans. Instrum. Meas.*, vol. 54, no. 5, pp. 1715–1720, Oct. 2005.

[33] Aeroflex. (2016). *PXI Modules 3030 Series RF Digitizers, Issue 23*. [Online]. Available: http://ats.aeroflex.com/support/technical-support/product-supportdocuments/3030-series

Zhe Li (S'16) received the B.S. degree in telecommunication engineering from the Nanjing University of Posts and Telecommunication, Nanjing, China, in 2011, and the M.S. degree in software engineering from Southeast University, Nanjing, in 2014, where he is currently pursuing the Ph.D. degree with the School of Information and Engineering. His current research interests include complex-valued statistical analysis and its applications on I/Q measurement.

Yili Xia (M'11) received the B.Eng. degree in information engineering from Southeast University, Nanjing, China, in 2006, and the M.Sc. degree (Hons.) in communications and signal processing from the Department of Electrical and Electronic Engineering, Imperial College London, London, U.K., in 2007, and the Ph.D. degree in adaptive signal processing from the Imperial College London in 2011.

Since 2013, he has been an Associate Professor with the School of Information and Engineering, Southeast University. His current research interests include complex-valued linear and nonlinear adaptive filters and complex-valued statistical analysis and their applications on communications.

Wenjiang Pei received the M.S. and Ph.D. degrees in instrumentation and measurement from the Nanjing University of Aeronautics and Astronautics, Nanjing, China, in 1995 and 1997, respectively.

He is currently a Professor with the School of Information and Engineering, Southeast University, Nanjing. His research interests signal processing and hardware instrumentation for communications.

Kai Wang received the Ph.D. degree in signal processing from the School of Information and Engineering, Southeast University, Nanjing, China, in 2009.

He is currently an Associate Professor in signal processing with Southeast University. His current research interests include parameter estimation and signal processing for communications.

Yongming Huang (M'10) received the B.S. and M.S. degrees from Nanjing University, Nanjing, China, in 2000 and 2003, respectively, and the Ph.D. degree in electrical engineering from Southeast University, Nanjing, in 2007.

Since 2007, he has been a Faculty Member with the School of Information Science and Engineering, Southeast University, where he is currently a Full Professor. From 2008 to 2009, he visited the Signal Processing Laboratory, School of Electrical Engineering, KTH Royal Institute of Technology, Stockholm, Sweden. His current research interests include multiple-antenna wireless communications and signal processing.

Dr. Huang serves as an Associate Editor of the IEEE TRANSACTIONS ON SIGNAL PROCESSING, the EURASIP *Journal on Advances in Signal Processing*, and the EURASIP *Journal on Wireless Communications and Networking*.

Danilo P. Mandic (M'99–SM'03–F'12) received the Ph.D. degree in nonlinear adaptive signal processing from the Imperial College London, London, U.K., in 1999.

He is currently a Professor in signal processing with the Imperial College London. He has been a Guest Professor with Katholieke Universiteit Leuven, Leuven, Belgium, the Tokyo University of Agriculture and Technology, Tokyo, Japan, and Westminster University, London, and a Frontier Researcher with RIKEN, Wako, Japan. He has authored the book *Recurrent Neural Networks for Prediction: Learning Algorithms, Architectures and Stability* (First Edition, 2001) and *Complex Valued Nonlinear Adaptive Filters: Noncircularity, Widely Linear and Neural Models* (First Edition, Wiley, 2009). He was an Editor of the book *Signal Processing Techniques for Knowledge Extraction and Information Fusion* (Springer, 2008) and over 200 publications on signal and image processing. His current research interest include in the area of nonlinear adaptive signal processing, multivariate data analysis, and nonlinear dynamics.

Dr. Mandic has been a member of the IEEE Technical Committee on Signal Processing Theory and Methods. He has been an Associate Editor of the *IEEE Signal Processing Magazine*, the IEEE TRANSACTIONS ON CIRCUITS AND SYSTEMS II, the IEEE TRANSACTIONS ON SIGNAL PROCESSING, the IEEE TRANSACTIONS ON NEURAL NETWORKS, and the *International Journal of Mathematical Modeling and Algorithms*. He has produced award winning papers and products resulting from his collaboration with industry.